Multiple-relaxation-time lattice-Boltzmann model for multiphase flow

Michael E. McCracken[1,*] and John Abraham[1]
[1]*Department of Mechanical Engineering, Purdue University, 500 Allison Road, West Lafayette, Indiana 47907*
(Received 13 May 2004; published 8 March 2005)

The lattice-Boltzmann method has shown promise in simulating multiphase flows. However, when using the Bhatnagar-Gross-Krook (BGK) collision operator and polynomial equilibria, numerical stability problems have been shown to occur as the relaxation time is decreased. Some authors have suggested the use of multiple-relaxation-time (MRT) models in lieu of the BGK collision operator, which employs a single relaxation time, to enhance numerical stability. In this paper, a MRT lattice-Boltzmann model for multiphase flow is developed and evaluated for accuracy in several test problems including oscillating liquid cylinders and capillary waves. It is shown that the MRT model is able to achieve numerically stable results at lower viscosities relative to the corresponding BGK model.

DOI: 10.1103/PhysRevE.71.036701 PACS number(s): 47.11.+j, 47.55.Kf

I. INTRODUCTION

One significant advantage of the lattice-Boltzmann method (LBM) over traditional Navier-Stokes computational methods is its ability to model multiphase flows based upon physics at a mesoscopic level [1–3]. Traditional front capturing methods such as level sets and volume of fluid (VOF) require interface reconstruction in order to determine the curvature of the interface and in turn the influence of surface tension on the fluid momentum [4]. Front tracking methods also use the curvature of the interface to add a surface force between liquids and gases [5]. The use of surface forces is a particular problem when trying to determine the curvature at a singular point on an interface as often occurs in liquid breakup. Therefore, the LBM is an attractive alternative.

However, when using the Bhathagar-Gross-Krook (BGK) collision operator, which has a single relaxation time, and a Taylor series expansion of the Maxwell-Boltzmann equilibrium distribution function for the equilibria, there exists a limitation. At low values of fluid viscosity, the method is numerically unstable. While the cause of the numerical instabilities in these lattice-Boltzmann models is still an open debate in the literature, some [6] have attributed them to the nonexistence of an H theorem. There exist two schools of thought on how to overcome numerical instabilities. The first [6–8] suggests using nonpolynomial equilibrium distribution functions, but these methods have been shown to dramatically increase the computational requirements [9] and sometimes lead to incorrect macroscopic equations [10]. The particular problem with entropic models is that the transport coefficients in these models are not constant, and they strongly depend on local velocity. The other school [11,12] promotes the use of multiple relaxation times in order to reduce the growth of numerical instabilities. In this work, we will adopt the latter approach.

In this paper, a multiple-relaxation-time (MRT) lattice Boltzmann model for multiphase flow is developed. Previous authors have suggested using a collision operator based upon multiple relaxation times for single-phase flows [11–13] and have shown increased numerical stability for such flows with proper tuning of the relaxation times. The use of MRT models for these flows allows for independent adjustment of bulk and shear viscosities and for nonunity Lewis numbers [11]. In this paper, a MRT lattice-Boltzmann model for multiphase flow is developed.

In Sec. II, a two-phase MRT lattice-Boltzmann model is developed. In Sec. III, the model is extended to an index function approach similar to He *et al.* [1]. The hydrodynamic equations corresponding to the lattice-Boltzmann model are derived in Sec. IV. In Sec. V, the model is evaluated for accuracy on several problems including oscillating liquid cylinders and capillary waves. The paper is concluded in Sec. VI.

II. TWO-PHASE, MULTIPLE-RELAXATION-TIME LATTICE-BOLTZMANN MODEL

The continuous Boltzmann equation with a forcing term is given by

$$\partial_t f + \boldsymbol{\xi} \cdot \boldsymbol{\nabla} f + \frac{\mathbf{F}}{\rho} \cdot \boldsymbol{\nabla}_{\xi} f = \boldsymbol{\Omega}_{coll}, \tag{1}$$

where f is the probability distribution function, $\boldsymbol{\xi}$ is the particle velocity, $\mathbf{F}$ is a forcing term, ρ is the density, and $\boldsymbol{\Omega}_{coll}$ is the change due to collisions. The gradient with respect to particle velocity in two-dimensional space can be approximated by [2]

$$\boldsymbol{\nabla}_{\xi} f \approx \boldsymbol{\nabla}_{\xi} f^{MB} = -\frac{(\boldsymbol{\xi} - \mathbf{u})}{RT} f^{MB}, \tag{2}$$

where f^{MB} is the Maxwell-Boltzmann distribution function, $\mathbf{u}$ is the macroscopic velocity, R is the gas constant, and T is the temperature. In order to convert Eq. (1) into an LBM model, the equation must be integrated in time. The advection terms are integrated along the characteristic directions and the collision and forcing terms are integrated using explicit Euler and trapezoidal methods, respectively. Then the equations are discretized into a velocity set. This yields the relationship [2]

*Electronic address: michael.e.mccracken@exxonmobil.com

$$f_\alpha(\mathbf{x}+\mathbf{e}_\alpha\delta_t,t+\delta_t)-f_\alpha(\mathbf{x},t)=\mathbf{\Omega}_{coll}\delta_t+\frac{\delta_t}{2}[f_\alpha^F(\mathbf{x}+\mathbf{e}_\alpha\delta_t,t+\delta_t)+f_\alpha^F(\mathbf{x},t)], \tag{3}$$

where

$$\mathbf{\Omega}_{coll}\delta_t=-\mathbf{\Lambda}(f-f^{eq}), \tag{4}$$

$$f_\alpha^F=\frac{\mathbf{F}\cdot(\mathbf{e}_\alpha-\mathbf{u})}{\rho RT}f_\alpha^{MB}. \tag{5}$$

In the BGK model [2], the relaxation matrix $\mathbf{\Lambda}$ is a diagonal matrix with elements of $1/\tau$, where τ is the dimensionless relaxation time. In the MRT model, the relaxation matrix will be a full matrix. The collision term in Eq. (3) is first order, but will result in second-order accuracy at the macroscopic level once numerical diffusion is incorporated into the viscosity. The method is overall first order in time and second order in space. The discretized velocity set $\mathbf{e}_\alpha$ is given by the following for the two-dimensional nine-velocity (D2Q9) model:

$$\mathbf{e}_\alpha=\begin{cases}(0,0), & \alpha=0,\\ \left(\cos\left(\frac{(\alpha-1)\pi}{2}\right),\sin\left(\frac{(\alpha-1)\pi}{2}\right)\right)c, & \alpha=1-4,\\ \sqrt{2}\left(\cos\left(\frac{(\alpha-5)\pi}{2}+\frac{\pi}{4}\right),\sin\left(\frac{(\alpha-5)\pi}{2}+\frac{\pi}{4}\right)\right)c, & \alpha=5-8,\end{cases} \tag{6}$$

where c is related to the lattice spacing by $c=\delta_x/\delta_t$. The speed of sound, c_s, is $c/\sqrt{3}$ and is related to the universal gas constant by $RT=c_s^2$. In Eq. (5), f_α^F represents the changes to the distribution function due to the forcing term $\mathbf{F}$. In this work, we use the mean-field approximation of van der Waals [14] to model the intermolecular attraction $\mathbf{F}_s$ and an exclusion volume term $\mathbf{F}_{ev}$ [15] to account for the increased probability of collision. Other authors have employed the same approach [1,2,16–18]. $\boldsymbol{F}$ may be written as

$$\mathbf{F}=\mathbf{F}_s+\mathbf{F}_{ev}=\kappa\rho\boldsymbol{\nabla}\nabla^2\rho-\boldsymbol{\nabla}\psi, \tag{6a}$$

where ψ is the nonideal part of the equation of state, $\psi=p-\rho RT$. In this work, the Carnahan-Starling equation of state [19] was employed—i.e.,

$$p(\rho)=\rho RT\frac{1+b\rho/4+(b\rho/4)^2-(b\rho/4)^3}{(1-b\rho/4)^3}-a\rho^2, \tag{7}$$

with $a=b=4$. Here p is the pressure. A Taylor series expansion of the Maxwell-Boltzmann distribution is used for equilibria and is given by

$$f_\alpha^{MB}=w_\alpha\rho\left[1+\frac{\mathbf{e}_\alpha\cdot\mathbf{u}}{RT}+\frac{(\mathbf{e}_\alpha\cdot\mathbf{u})^2}{2(RT)^2}-\frac{\mathbf{u}\cdot\mathbf{u}}{2RT}\right], \tag{8}$$

where $w_\alpha=4/9$ for $\alpha=0$, $w_\alpha=1/9$ for $\alpha=1-4$, and $w_\alpha=1/36$ for $\alpha=5-8$. Equation (3) is implicit. In order to maintain an explicit scheme the following variable is introduced:

$$\overline{f}_\alpha=f_\alpha-\frac{1}{2}f_\alpha^F\delta_t. \tag{9}$$

Using Eq. (9), Eq. (3) is rewritten as

$$\overline{f}_\alpha(\mathbf{x}+\mathbf{e}_\alpha\delta_t,t+\delta_t)=\overline{f}_\alpha(\mathbf{x},t)-\sum_i\mathbf{\Lambda}_{\alpha i}(\overline{f}_i-f_i^{eq})+\delta_t f_\alpha^F-\frac{1}{2}\delta_t\sum_i\mathbf{\Lambda}_{\alpha i}f_i^F. \tag{10}$$

This equation can be mapped onto moment space by multiplying through by a transformation matrix $\mathbf{T}$ to obtain

$$\hat{\overline{f}}_\alpha(\mathbf{x}+\mathbf{e}_\alpha\delta_t,t+\delta_t)=\hat{\overline{f}}_\alpha(\mathbf{x},t)-\sum_i\hat{\mathbf{\Lambda}}_{\alpha i}(\hat{\overline{f}}_i-\hat{f}_i^{eq})+\delta_t\hat{f}_\alpha^F-\frac{1}{2}\delta_t\sum_i\hat{\mathbf{\Lambda}}_{\alpha i}\hat{f}_i^F, \tag{11}$$

where $\hat{\overline{f}}=\mathbf{T}\overline{f}$, $\hat{\mathbf{\Lambda}}=\mathbf{T}\mathbf{\Lambda}\mathbf{T}^{-1}$, and $\hat{f}^F=\mathbf{T}f^F$. The transformation matrix used in this work is similar to that employed by Lallemand and Luo [11] and has the form

$$\mathbf{T}^T=[\langle\rho|,\langle e|,\langle e^2|,\langle j_x|,\langle q_x|,\langle j_y|,\langle q_y|,\langle p_{xx}|,\langle p_{xy}|], \tag{12}$$

where

$$|\rho\rangle=|\mathbf{e}_\alpha|^0, \tag{13a}$$

$$|e\rangle_\alpha=-4|\mathbf{e}_\alpha|^0+3(e_{\alpha,x}^2+e_{\alpha,y}^2), \tag{13b}$$

$$|e^2\rangle_\alpha=4|\mathbf{e}_\alpha|^0-\frac{21}{2}(e_{\alpha,x}^2+e_{\alpha,y}^2)+\frac{9}{2}(e_{\alpha,x}^2+e_{\alpha,y}^2)^2, \tag{13c}$$

$$|j_x\rangle_\alpha=e_{\alpha,x}, \tag{13d}$$

$$|q_x\rangle_\alpha=[-5|\mathbf{e}_\alpha|^0+3(e_{\alpha,x}^2+e_{\alpha,y}^2)]e_{\alpha,x}, \tag{13e}$$

$$|j_y\rangle_\alpha = e_{\alpha,y}, \tag{13f}$$

$$|q_y\rangle_\alpha = [-5|\mathbf{e}_\alpha|^0 + 3(e_{\alpha,x}^2 + e_{\alpha,y}^2)]e_{\alpha,y}, \tag{13g}$$

$$|p_{xx}\rangle_\alpha = e_{\alpha,x}^2 - e_{\alpha,y}^2, \tag{13h}$$

$$|p_{xy}\rangle_\alpha = e_{\alpha,x}e_{\alpha,y}. \tag{13i}$$

For the case where $c=1$, Eq. (12) yields

$$\mathbf{T} = \begin{bmatrix} 1 & 1 & 1 & 1 & 1 & 1 & 1 & 1 & 1 \\ -4 & -1 & -1 & -1 & -1 & 2 & 2 & 2 & 2 \\ 4 & -2 & -2 & -2 & -2 & 1 & 1 & 1 & 1 \\ 0 & 1 & 0 & -1 & 0 & 1 & -1 & -1 & 1 \\ 0 & -2 & 0 & 2 & 0 & 1 & -1 & -1 & 1 \\ 0 & 0 & 1 & 0 & -1 & 1 & 1 & -1 & -1 \\ 0 & 0 & -2 & 0 & 2 & 1 & 1 & -1 & -1 \\ 0 & 1 & -1 & 1 & -1 & 0 & 0 & 0 & 0 \\ 0 & 0 & 0 & 0 & 0 & 1 & -1 & 1 & -1 \end{bmatrix}. \tag{14}$$

The equilibrium in moment space, $\hat{f}^{eq}$, is given by

$$\hat{f}^{eq\ T} = [\rho, e^{eq}, e^{2\ eq}, j_x, q_x^{eq}, j_y, q_y^{eq}, p_{xx}^{eq}, p_{xy}^{eq}], \tag{15}$$

where ρ is the density, j_x and j_y are the momentum fluxes—i.e., $j_x=\rho u_x$—and the equilibrium values can be found from the expressions

$$e^{eq} = \frac{1}{4}\alpha_2\rho + \frac{1}{6}\gamma_2(j_x^2 + j_y^2)/\rho, \tag{16a}$$

$$e^{2\ eq} = \frac{1}{4}\alpha_3\rho + \frac{1}{6}\gamma_4(j_x^2 + j_y^2)/\rho, \tag{16b}$$

$$q_x^{eq} = \frac{1}{2}c_1 j_x, \tag{16c}$$

$$q_y^{eq} = \frac{1}{2}c_1 j_y, \tag{16d}$$

$$p_{xx}^{eq} = \frac{3}{2}\gamma_1(j_x^2 - j_y^2)/\rho, \tag{16e}$$

$$p_{xy}^{eq} = \frac{3}{2}\gamma_3(j_x j_y)/\rho. \tag{16f}$$

In this work, the constants in Eqs. (16a) and (16b) are $\alpha_2=-8$, $\alpha_3=4$, $c_1=-2$, $\gamma_1=\gamma_3=2/3$, $\gamma_2=18$, and $\gamma_4=-18$. These values give the correct hydrodynamic equations as shown in Sec. IV. It can be easily shown that the above choice of constants yields equilibria that are equivalent to a Taylor series expansion of the Maxwell-Boltzmann equilibrium distribution function in velocity space—i.e.,

$$f^{eq} = \mathbf{T}^{-1}\hat{f}^{eq} = f^{MB}. \tag{17}$$

The relaxation matrix $\hat{\mathbf{\Lambda}}$ in moment space, which appears in Eq. (11), is a diagonal matrix given by

$$\hat{\mathbf{\Lambda}} = \mathrm{diag}[s_1, s_2, s_3, s_4, s_5, s_6, s_7, s_8, s_9], \tag{18}$$

whose elements represent the inverse of the relaxation time for the transformed distribution function $\hat{f}$ as it is relaxed to the equilibrium distribution function in moment space, $\hat{f}^{eq}$. Even though the values of ρ, j_x, and j_y do not change in the relaxation process, the values of s_1, s_4, and s_6 should be nonzero in order to maintain the influence of the trapezoidal integration in Eq. (3). Notice that, for example, irrespective of the value of s_1, $s_1(\rho-\rho)=0$. For equal weighting at both the current time and location and the subsequent time and location, $s_1=s_4=s_6=1$. In this work, $s_2=1.64$, $s_3=1.54$, $s_5=s_7=1.7$, and $s_8=s_9=1/\tau$, where τ is the relaxation time in the BGK model and related to the viscosity by

$$\nu = \left(\tau - \frac{1}{2}\right)c_s^2\delta_t, \tag{19}$$

as demonstrated in Sec. IV. The macroscopic properties can be found from the summations

$$\rho = \sum_\alpha f_\alpha = \sum_\alpha \overline{f_\alpha}, \tag{20}$$

$$\rho\mathbf{u} = \sum_\alpha f_\alpha \mathbf{e}_\alpha = \sum_\alpha \overline{f}_\alpha \mathbf{e}_\alpha + \frac{1}{2}\mathbf{F}\delta_t, \tag{21}$$

which are analogous to $\rho=\hat{f}_1=\hat{\overline{f}}_1$, $\rho u_x=\hat{f}_4=\hat{\overline{f}}_4+\frac{1}{2}\delta_t\hat{f}_4^F$, and $\rho u_y=\hat{f}_6=\hat{\overline{f}}_6+\frac{1}{2}\delta_t\hat{f}_6^F$. The property of surface tension is dependent on the constant κ in Eq. (6), which determines the magnitude of the force. Zhang *et al.* [18] have used the following integral relationship to analytically relate surface tension σ and κ:

$$\sigma = \kappa I(a) = \kappa\int_{-\infty}^{\infty}\left(\frac{\partial\rho}{\partial z}\right)^2 dz, \tag{22}$$

where z is a direction normal to a flat interface.

The model discussed in this section satisfies the correct hydrodynamic equations for two-phase, viscous flow. However, the model is prone to numerical instabilities. These include unexpected phase change—i.e., liquid condensation—when relatively large forces are applied such as with gravity in Rayleigh-Taylor instabilities. Also, the model is inconvenient to apply when the liquid and gas densities are changed because the equation of state must be altered for each scenario. This is accomplished by selecting new values of a and b. To overcome these challenges, we extend this model to an index function approach similar to that of He *et al.* [1] in the next section. In this approach, the governing equations are limited to psuedoincompressible flow where each phase is nearly incompressible. This helps eliminate some of the numerical instabilities due to undesired phase change. The use of an index function allows for independent adjustment of

the liquid and gas densities from the equation of state. The index function is required to follow the equation of state.

III. INDEX FUNCTION, TWO-PHASE, MRT LATTICE-BOLTZMANN MODEL

In the index function model, two different distribution functions h and g are employed: one, h, to track the location of the liquid in a manner similar to level sets or VOF and the other, g, to determine the macroscopic properties of pressure and momentum. There are two major advantages to using an index function model [1]. First, nearly incompressible two-phase flow can be simulated by forcing the material derivative of ψ to be zero. This reduces fluctuations in the liquid density, which is often observed in other lattice-Boltzmann models. Second, the numerical stability of the model can be enhanced by using the pressure distribution function to calculate the velocity field. The numerical calculation of $\nabla\psi(\rho)$ can lead to large errors at an interface. When using a pressure distribution function, $\nabla\psi(\rho)$ is multiplied by a small parameter of the order of the Mach number. This reduces the effects of numerical perturbations associated with calculation errors.

The indexing distribution function h is used to track the location of the liquid and gas and, therefore, only needs to reproduce the correct hydrodynamic equation for continuity. It has been shown [1] that in the Chapman-Enskog expansion the surface tension force does not factor into the derivation of the continuity equation. The governing equation for the indexing distribution function is given by

$$\overline{h_\alpha}(\mathbf{x}+\mathbf{e}_\alpha\delta_t,t+\delta_t)=\overline{h_\alpha}(\mathbf{x},t)-\sum_i \mathbf{\Lambda}_{\alpha i}(\overline{h_i}(\mathbf{x},t)-h_i^{eq}(\mathbf{x},t)) + \delta_t h^F-\frac{1}{2}\delta_t\sum_i \mathbf{\Lambda}_{\alpha i}h_i^F, \tag{23}$$

where

$$h_\alpha^F=-\frac{(\mathbf{e}_\alpha-\mathbf{u})}{c_s^2}\cdot\nabla\psi(\phi)\mathbf{\Gamma}_\alpha(\mathbf{u}), \tag{24}$$

$$\mathbf{\Gamma}_\alpha(\mathbf{u})=\frac{f_\alpha^{MB}}{\rho}. \tag{25}$$

The distributions h_α define the indexing function ϕ by $\phi=\Sigma_\alpha h_\alpha$. The index function ϕ is related to the density by interpolation. Notice that ψ is a function of ϕ for this forcing term. We have employed a linear interpolation to determine ρ—i.e.,

$$\rho(\phi)=\rho_g+\frac{\phi-\phi_g}{\phi_l-\phi_g}(\rho_l-\rho_g), \tag{26}$$

where ϕ_l and ϕ_g are the upper and lower limits for the index function and ρ_l and ρ_g are the liquid and gas densities, respectively. The theoretical limits for the index function ϕ can be determined by Maxwell's equal-area rule [1]. However, these should be calculated numerically in order to determine the equilibrium values of these limits. This is further discussed in Sec. V.

The second distribution function determines the evolution of the pressure and can be derived from the density distribution function f by applying the following transformation to Eq. (1) [1]:

$$g=fRT+\psi(\rho)\Gamma(0), \tag{27}$$

and assuming [1]

$$\frac{D\psi(\rho)}{Dt}=(\xi-\mathbf{u})\cdot\nabla\psi(\rho). \tag{28}$$

Using an explicit Euler integration on the collision term and a trapezoidal integration on the forcing term, the pressure evolution equation becomes

$$g_\alpha(\mathbf{x}+\mathbf{e}_\alpha\delta_t,t+\delta_t)=g_\alpha(\mathbf{x},t)-\sum_i \mathbf{\Lambda}_{\alpha i}[g_i(\mathbf{x},t)-g_i^{eq}(\mathbf{x},t)] + \delta_t g_\alpha^F|_{(\mathbf{x},t)}+\delta_t g_\alpha^F|_{(\mathbf{x}+\mathbf{e}_\alpha\delta_t,t+\delta_t)}, \tag{29}$$

where

$$g_\alpha^F=(\mathbf{e}_\alpha-\mathbf{u})\cdot\{\mathbf{\Gamma}_\alpha(\mathbf{u})\mathbf{F}_s-[\mathbf{\Gamma}_\alpha(\mathbf{u})-w_\alpha]\nabla\psi(\rho)\}, \tag{30}$$

and g_α^{eq} is the equilibrium in velocity space. Equation (29) can be transformed into an explicit form by solving for $\overline{g_\alpha}$ where

$$\overline{g_\alpha}=g_\alpha-\frac{1}{2}g_\alpha^F\delta_t. \tag{31}$$

This gives

$$\overline{g_\alpha}(\mathbf{x}+\mathbf{e}_\alpha\delta_t,t+\delta_t)=\overline{g_\alpha}(\mathbf{x},t)-\sum_i \mathbf{\Lambda}_{\alpha i}[\overline{g_i}(\mathbf{x},t)-g_i^{eq}(\mathbf{x},t)] + \delta_t g_\alpha^F-\frac{1}{2}\delta_t\sum_i \mathbf{\Lambda}_{\alpha i}g_i^F. \tag{32}$$

Equations (23) and (32) can be transformed into moment space by multiplying through by the transformation matrix $\mathbf{T}$ to obtain

$$\hat{\overline{h_\alpha}}(\mathbf{x}+\mathbf{e}_\alpha\delta_t,t+\delta_t)=\hat{\overline{h_\alpha}}(\mathbf{x},t)-\sum_i \hat{\mathbf{\Lambda}}_{\alpha i}[\hat{\overline{h_i}}(\mathbf{x},t)-\hat{h}_i^{eq}(\mathbf{x},t)] + \delta_t\hat{h}_\alpha^F-\frac{1}{2}\delta_t\sum_i \hat{\mathbf{\Lambda}}_{\alpha i}\hat{h}_i^F, \tag{33}$$

$$\hat{\overline{g_\alpha}}(\mathbf{x}+\mathbf{e}_\alpha\delta_t,t+\delta_t)=\hat{\overline{g_\alpha}}(\mathbf{x},t)-\sum_i \hat{\mathbf{\Lambda}}_{\alpha i}[\hat{\overline{g_i}}(\mathbf{x},t)-\hat{g}_i^{eq}(\mathbf{x},t)] + \delta_t\hat{g}_\alpha^F-\frac{1}{2}\delta_t\sum_i \hat{\mathbf{\Lambda}}_{\alpha i}\hat{g}_i^F. \tag{34}$$

The equilibria in moment space are

$$\hat{g}^{eq}=RT\hat{f}^{eq}+\psi(\rho)\hat{\mathbf{\Gamma}}(0), \tag{35}$$

$$\hat{h}^{eq} = \frac{\phi}{\rho}\hat{f}^{eq}. \tag{36}$$

The value of the index function is related to the macroscopic property of density by interpolation as shown in Eq. (26) and by definition is

$$\phi = \sum_{\alpha} \overline{h}_{\alpha}. \tag{37}$$

The pressure and velocity are found from the moments of the pressure distribution function—i.e.,

$$p = \sum_{\alpha} \overline{g}_{\alpha} - \frac{1}{2}\mathbf{u}\cdot\boldsymbol{\nabla}\psi(\rho)\delta_t, \tag{38}$$

$$\rho RT\mathbf{u} = \sum_{\alpha} \mathbf{e}_{\alpha}\overline{g}_{\alpha} + \frac{RT}{2}\mathbf{F}_s\delta_t. \tag{39}$$

One possible solution procedure is to calculate the moments by employing Eqs. (16a)–(16f) using the density and velocity which are either given as initial conditions or calculated during the previous time step. Then, in order to find the equilibrium values of g and h in moment space use Eq. (15) along with Eqs. (35) and (36). The contributions due to surface tension forces are found from Eqs. (24) and (30). The values of the distribution functions at the next time step are found using Eqs. (33) and (34). These values are then employed to find the density and velocities at this time step using Eqs. (26), (37), and (39).

IV. HYDRODYNAMIC EQUATIONS

It is of interest to determine the macroscopic equations corresponding to the discretized Boltzmann equations for the MRT model. In this section, Chapman-Enskog expansion terms are employed to find these equations. We use the distribution function f in this analysis because the derivation is more straightforward and the distribution function g is related to f via the transformation in Eq. (27). A similar derivation could be performed using distribution functions h and g. In fact, this has been previously performed by Zhang [20] for the index function model of He *et al.* [1]. In his work [20], the momentum equation is derived in terms of the pressure and is analogous to the momentum equation derived here, but the continuity equation contains a source term, which is nonzero when ϕ is not equal to ρ. The exact derivation of this source term is not clear since it involves estimating the first-order expansion of the distribution function h. Therefore, we perform this analysis using the distribution function f and start with the expansions

$$f_{\alpha}(\mathbf{x}+\mathbf{e}_{\alpha}\delta_t, t+\delta_t) = \sum_{n=0} \varepsilon^n (\partial_t + \mathbf{e}_{\alpha}\cdot\boldsymbol{\nabla})^n f_{\alpha}(\mathbf{x},t), \tag{40a}$$

$$f_{\alpha} = \sum_{n=0} \varepsilon^n f_{\alpha}^{(n)}, \tag{40b}$$

$$\partial_t = \sum_{n=0} \varepsilon^n \partial_{t_n}. \tag{40c}$$

Appling the expansions in Eq. (40) to Eq. (3), we get the following relationship for the zeroth; first; and second-order expansions in ε:

$$f_{\alpha}^{(0)} = f_{\alpha}^{eq}, \tag{41a}$$

$$(\partial_{t_0} + \mathbf{e}_{\alpha}\cdot\boldsymbol{\nabla})f_{\alpha}^{(0)} = -\sum_i \boldsymbol{\Lambda}_{\alpha i} f_i^{(1)} + f_{\alpha}^{F}, \tag{41b}$$

$$\partial_{t_1} f_{\alpha}^{(0)} + (\partial_{t_0} + \mathbf{e}_{\alpha}\cdot\boldsymbol{\nabla})\left(f_{\alpha}^{(1)} - \frac{1}{2}\sum_i \boldsymbol{\Lambda}_{\alpha i} f_i^{(1)}\right) = -\sum_i \boldsymbol{\Lambda}_{\alpha i} f_i^{(2)}. \tag{41c}$$

These can be easily converted into moment space to obtain

$$\hat{f}^{(0)} = \hat{f}^{(eq)}, \tag{42a}$$

$$(\partial_{t_0} + \hat{\mathbf{E}}_i\partial_i)\hat{f}^{(0)} = -\hat{\boldsymbol{\Lambda}}\hat{f}^{(1)} + \hat{f}^{F}, \tag{42b}$$

$$\partial_{t_1}\hat{f}^{(0)} + (\partial_{t_0} + \hat{\mathbf{E}}_i\partial_i)\left(\mathbf{I} - \frac{1}{2}\hat{\boldsymbol{\Lambda}}\right)\hat{f}^{(1)} = -\hat{\boldsymbol{\Lambda}}\hat{f}^{(2)}, \tag{42c}$$

where $\hat{\mathbf{E}}_i = \mathbf{T}(e_{\alpha i}\mathbf{I})$ and

$$\hat{f}^{(1)T} = [0, e^{(1)}, e^{2(1)}, 0, q_x^{(1)}, 0, q_y^{(1)}, p_{xx}^{(1)}, p_{xy}^{(1)}]. \tag{43}$$

Writing out the equations of Eq. (42b) the following equations are obtained:

$$\partial_{t_0}\rho + \partial_x j_x + \partial_y j_y = 0, \tag{44a}$$

$$\partial_{t_0}[-2\rho + 3(j_x^2 + j_y^2)/\rho] = -s_2 e^{(1)} + 6u_x F_x + 6u_y F_y, \tag{44b}$$

$$\partial_{t_0}[\rho - 3(j_x^2 + j_y^2)/\rho] - \partial_x j_x - \partial_y j_y = -s_3 e^{2(1)} - 6u_x F_x - 6u_y F_y, \tag{44c}$$

$$\partial_{t_0} j_x + \partial_x\left[\frac{1}{3}\rho + \frac{j_x^2}{\rho}\right] + \partial_y[j_x j_y/\rho] = F_x, \tag{44d}$$

$$-\partial_{t_0} j_x + \partial_x\left[-\frac{1}{3}\rho + \frac{-j_x^2 + j_y^2}{\rho}\right] + \partial_y[j_x j_y/\rho] = -s_5 q_x^{(1)} - F_x, \tag{44e}$$

$$\partial_{t_0} j_y + \partial_x[j_x j_y/\rho] + \partial_y\left[\frac{1}{3}\rho + \frac{j_y^2}{\rho}\right] = F_y, \tag{44f}$$

$$-\partial_{t_0} j_y + \partial_x[j_x j_y/\rho] + \partial_y\left[-\frac{1}{3}\rho + \frac{j_x^2 - j_y^2}{\rho}\right] = -s_7 q_y^{(1)} - F_y, \tag{44g}$$

$$\partial_{t_0}[(j_x^2 - j_y^2)/\rho] + \frac{2}{3}\partial_x j_x - \frac{2}{3}\partial_y j_y = -s_8 p_{xx}^{(1)} + 2u_x F_x - 2u_y F_y, \tag{44h}$$

$$\partial_{t_0}[j_x j_y/\rho] + \frac{1}{3}\partial_x j_y + \frac{1}{3}\partial_y j_x = -s_9 p_{xy}^{(1)} + u_y F_x + u_x F_y. \tag{44i}$$

Now writing out the equations for the conserved moments of Eq. (42c), the following are obtained:

$$\partial_{t_1}\rho = 0, \tag{45a}$$

$$\partial_{t_1} j_x + \partial_x\left[\frac{1}{6}\left(1 - \frac{1}{2}s_2\right)e^{(1)} + \frac{1}{2}\left(1 - \frac{1}{2}s_8\right)p_{xx}^{(1)}\right] + \partial_y\left[\left(1 - \frac{1}{2}s_9\right)p_{xy}^{(1)}\right] = 0, \tag{45b}$$

$$\partial_{t_1} j_y + \partial_x\left[\left(1 - \frac{1}{2}s_9\right)p_{xy}^{(1)}\right] + \partial_y\left[\frac{1}{6}\left(1 - \frac{1}{2}s_2\right)e^{(1)} - \frac{1}{2}\left(1 - \frac{1}{2}s_8\right)p_{xx}^{(1)}\right] = 0. \tag{45c}$$

Adding Eq. (44a) and ε times Eq. (45a) yields the continuity equation

$$\partial_t \rho + \partial_x j_x + \partial_y j_y = 0. \tag{46}$$

Adding Eq. (44d) and ε times Eq. (45b) and substituting for $p_{xx}^{(1)}$ and $p_{xy}^{(1)}$ using Eqs. (44h) and (44i), the following equation is obtained:

$$\begin{aligned}\partial_t j_x + \partial_x\left(\frac{1}{3}\rho + j_x^2/\rho\right) + \partial_y(j_x j_y/\rho) &= F_x - \varepsilon\frac{1}{6}\left(1 - \frac{1}{2}s_2\right)\partial_x e^{(1)} - \varepsilon\frac{1}{2}\left(1 - \frac{1}{2}s_8\right)\frac{1}{s_8}\partial_x \\ &\times\left[2u_x F_x - 2u_y F_y - \partial_{t_0}\left(\frac{j_x^2 - j_y^2}{\rho}\right) - \frac{2}{3}\partial_x j_x + \frac{2}{3}\partial_y j_y\right] \\ &- \varepsilon\left(1 - \frac{1}{2}s_9\right)\frac{1}{s_9}\partial_y\left[u_y F_x + u_x F_y - \partial_{t_0}\left(\frac{j_x j_y}{\rho}\right) - \frac{1}{3}\partial_x j_y - \frac{1}{3}\partial_y j_x\right].\end{aligned} \tag{47}$$

Adding Eq. (44f) and ε times Eq. (45c) and substituting for $p_{xx}^{(1)}$ and $p_{xy}^{(1)}$ using Eqs. (44h) and (44i), the following equation is obtained:

$$\begin{aligned}\partial_t j_y + \partial_x(j_x j_y/\rho) + \partial_y\left(\frac{1}{3}\rho + j_y^2/\rho\right) &= F_y - \varepsilon\frac{1}{6}\left(1 - \frac{1}{2}s_2\right)\partial_y e^{(1)} + \varepsilon\frac{1}{2}\left(1 - \frac{1}{2}s_8\right)\frac{1}{s_8}\partial_x \\ &\times\left[2u_x F_x - 2u_y F_y - \partial_{t_0}\left(\frac{j_x^2 - j_y^2}{\rho}\right) - \frac{2}{3}\partial_x j_x + \frac{2}{3}\partial_y j_y\right] \\ &- \varepsilon\left(1 - \frac{1}{2}s_9\right)\frac{1}{s_9}\partial_y\left[u_y F_x + u_x F_y - \partial_{t_0}\left(\frac{j_x j_y}{\rho}\right) - \frac{1}{3}\partial_x j_y - \frac{1}{3}\partial_y j_x\right].\end{aligned} \tag{48}$$

In order to evaluate the order of the term $\varepsilon\partial_x e^{(1)}$, we rearrange Eq. (44b) and use Eq. (44a) to determine $\partial_{t_0}\rho$, which gives

$$e^{(1)} = \frac{1}{s_2}\left[6u_x F_x + 6u_y F_y - 2(\partial_x j_x + \partial_y j_y) - 3\partial_{t_0}\left(\frac{j_x^2 + j_y^2}{\rho}\right)\right]. \tag{49}$$

Expanding the terms $\partial_{t_0} j_x^2$ and $\partial_{t_0} j_y^2$ and using Eqs. (44d) and (44f), while ignoring terms of order Ma^3, yields

$$\partial_{t_0}\left(\frac{j_x^2}{\rho}\right) = 2u_x\left[-\partial_x\left(\frac{1}{3}\rho + \frac{j_x^2}{\rho}\right) - \partial_y\left(\frac{j_x j_y}{\rho}\right) + F_x\right], \tag{50}$$

$$\partial_{t_0}\left(\frac{j_y^2}{\rho}\right) = 2u_y\left[-\partial_y\left(\frac{1}{3}\rho + \frac{j_y^2}{\rho}\right) - \partial_x\left(\frac{j_x j_y}{\rho}\right) + F_y\right]. \tag{51}$$

Using Eqs. (50) and (51) and ignoring higher-order terms of the form $u_x\partial_x(u_x j_x)$, Eq. (49) can be written as

$$e^{(1)} = \frac{1}{s_2}[-2\partial_x j_x - 2\partial_y j_y]. \tag{52}$$

Equation (52) can be shown to be small in the incompressible limit making this term negligible, but we shall retain this term to illustrate how the constant s_2 is related to the bulk viscosity. Similarly, reduced forms can be determined for $p_{xx}^{(1)}$ and $p_{xy}^{(1)}$—i.e.,

$$p_{xx}^{(1)} = \frac{1}{s_8}\left[-\partial_x\left(\frac{2}{3}j_x\right) + \partial_y\left(\frac{2}{3}j_y\right)\right], \tag{53}$$

$$p_{xy}^{(1)} = \frac{1}{s_9}\left[-\partial_x\left(\frac{1}{3}j_y\right) - \partial_y\left(\frac{1}{3}j_x\right)\right]. \tag{54}$$

These terms cannot be neglected because the $1/3$ factor represents the nondimensional speed of sound, $c_s^2 = 1/3$, which decreases the order of the terms. Now Eqs. (47) and (48) can be rewritten as the following using $s_8 = s_9 = 1/\tau$ and substituting in for F_x and F_y:

$$\partial_t j_x + j_x\partial_x u_x + j_y\partial_y u_x = -\partial_x p + \kappa\rho\partial_x\nabla^2\rho + \nu\nabla^2 j_x + \zeta\partial_x(\partial_x j_x + \partial_y j_y), \tag{55}$$

$$\partial_t j_y + j_x\partial_x u_y + j_y\partial_y u_y = -\partial_y p + \kappa\rho\partial_y\nabla^2\rho + \nu\nabla^2 j_y + \zeta\partial_y(\partial_x j_x + \partial_y j_y), \tag{56}$$

where $\varepsilon = \delta_t$, $1/3 = c_s^2$,

$$\nu = c_s^2\delta_t\left(\tau - \frac{1}{2}\right), \tag{57}$$

$$\zeta = c_s^2\delta_t\left(\frac{1}{s_2} - \frac{1}{2}\right), \tag{58}$$

$$p = c_s^2 \rho + \psi(\rho). \tag{59}$$

V. EVALUATION OF THE MODEL

The first step in evaluating the model is to determine the index function limits ϕ_l and ϕ_g and determine the value of $I(a)$ in Eq. (22). Both of these can be obtained by solving a "two-layer" problem where initially the fluids at two different densities are separated by a horizontal boundary in a domain with periodic boundary conditions on the sides and infinite boundary conditions on the top and bottom. The values of ϕ_l and ϕ_g from Maxwell's equal-area rule should be used as initial values for the index function of the corresponding fluid. The fluid is allowed to come equilibrium. Then, the value of $I(a)$ can be determined by the numerical integration of ϕ along the direction perpendicular to the interface according to Eq. (22). The equilibrium values will depend on the numerical scheme employed for calculating the gradient and Laplacian terms in Eqs. (6), (24), and (29). The results from this model and other two-phase LBM models have shown a large dependence on numerical schemes [21]. We have found that the use of a hybrid scheme for calculating gradients produces desirable results for a wide range of surface tension and viscosity values. In this work, the Laplacian is computed using a nine-point stencil—i.e.,

$$\nabla^2 \phi = \frac{1}{6\delta_x^2}[\phi_{(i+1,j+1)} + \phi_{(i+1,j-1)} + \phi_{(i-1,j+1)} + \phi_{(i-1,j-1)} + 4\phi_{(i,j+1)} + 4\phi_{(i,j-1)} + 4\phi_{(i+1,j)} + 4\phi_{(i-1,j)} - 20\phi_{(i,j)}]. \tag{60}$$

The gradients are calculated using a hybrid method where the sixth-order central difference method gets 75% weighting and is given by

$$\partial_i \psi = \frac{1}{60\delta_x}[-\psi_{(i-3,j)} + 9\psi_{(i-2,j)} - 45\psi_{(i-1,j)} + 45\psi_{(i+1,j)} - 9\psi_{(i+2,j)} + \psi_{(i+3,j)}]. \tag{61}$$

A 25% weighting is given to a fourth-order method based upon Taylor series expansions in velocity space—i.e.,

$$\partial_i \psi = \frac{1}{36c\delta_x} \sum_{\alpha=1}^{8} e_{\alpha,i}[8\psi(\mathbf{x} + \mathbf{e}_\alpha \delta_t) - \psi(\mathbf{x} + 2\mathbf{e}_\alpha \delta_t)]. \tag{62}$$

For the hybrid scheme the equilibrium values of the index function limits are $\phi_g = 0.022\,55$ and $\phi_l = 0.250\,08$, and $I(4) = 0.0152$ based upon computations of the "two-layer" problem with a $a=b=4$ in Eq. (7).

The surface tension predicted by Eq. (22) can be compared to the results of a numerical experiment [22–25]. A computational domain of 200×200 with periodic boundary conditions is set up with a two-dimensional (2D) "drop" in the middle of the domain with $\kappa = 0.1$, which corresponds to a surface tension of 0.001 52. Four different size drops are employed with radii of approximately 20, 30, 40, and 50. After the liquid drop reaches equilibrium the surface tension is calculated from Laplace's law $\sigma/r = (p_{in} - p_{out})$. Figure 1 compares the analytical pressure difference from Laplace's law to that computed by the MRT model. The largest error compared to theoretical value is 12% at $1/r = 0.025$ while the other errors are under 6%.

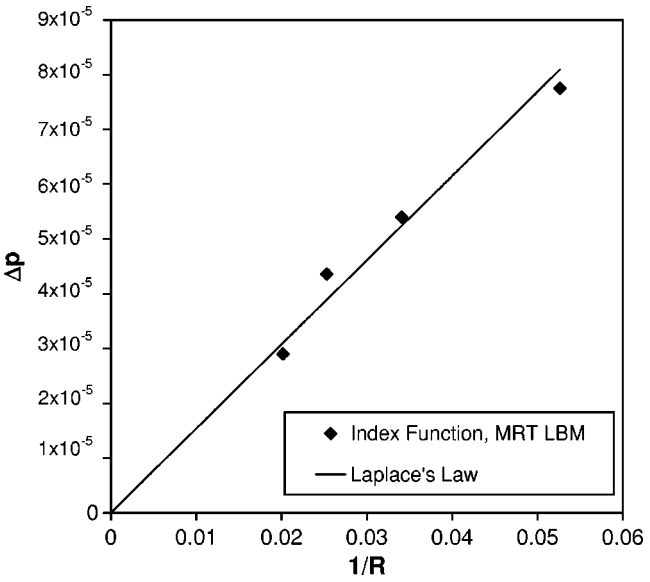

FIG. 1. Pressure change due to surface tension versus the inverse of radius for a 2D "drop."

Next, the index function MRT model is employed to solve an oscillating liquid cylinder problem. An initial elliptical cross section is given to the liquid with $\kappa = 0.05$, 0.1, and 0.2 and liquid densities of 0.2 and 1. The density ratio is 10, and the viscosity is 0.006 75 for all computations. Figure 2 illustrates the amplitude of the oscillations with dimensionless time for $\kappa = 0.2$ and $\rho_l = 0.2$. Lamb [26] performed an analytical study of an invisid liquid cylinder oscillating without the influence of an ambient gas. The frequency of oscillation predicted by Lamb [26] is given by

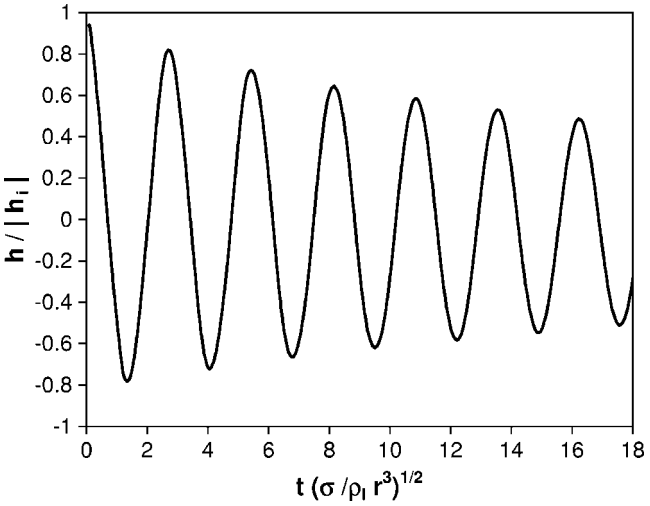

FIG. 2. Amplitude of oscillation versus time for a liquid cylinder ($\rho_l = 0.2, \sigma = 0.003\,04, \nu = 0.006\,75$).

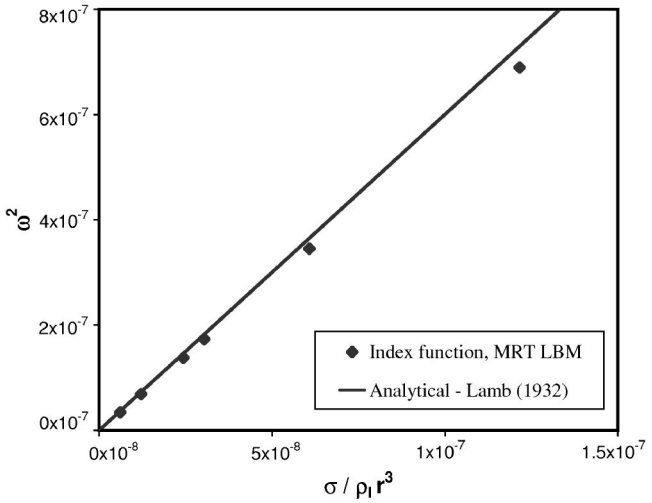

FIG. 3. Comparison of computed oscillation frequencies to those predicted by Lamb [26] for liquid cylinders with initially elliptic cross sections.

$$\omega^2 = n(n^2 - 1)\frac{\sigma}{\rho_l r^3}, \tag{63}$$

where $n=2$ for an initially elliptical cross section and r is the equilibrium radius. Figure 3 compares the analytical solution of Lamb to the oscillation frequencies obtained from the computations. All of the oscillation frequencies are approximately 3% lower than their corresponding analytical values. More accurate solutions are expected for computations with higher density ratios since the analytical solution is for oscillations without an ambient fluid. However, higher density ratios were not numerically stable for the viscosity employed ($\nu=0.006\,75$). This limitation on density ratio is not a problem specific to the work here, but is well recognized as one of the challenges with the LBM methods for two-phase flow. Premnath [27] has suggested that the numerical instability associated with the LBM at higher density ratios is related the pseudocompressible nature of the method. This appears to cause small fluctuations in density to lead to fluctuations in velocity, which in turn lead to instabilities. The use of multiple relaxation times may increase the sensitivity of the density ratio to numerical stability.

The index function, MRT model is also employed to simulate capillary waves with a small amplitude and long wavelength. Other authors [18,25] have performed similar numerical experiments. Initially, a sinusoidal perturbation with an amplitude of 5% of the wavelength is given to a liquid. Under the influence of surface tension, the wave oscillates with a decaying amplitude due to viscosity until the fluid is at rest. Chandrasekhar [28] derived an analytical solution for the oscillation frequency and decay rate of wave amplitude. The solution involves finding the roots of the equation

$$y^4 + 4\alpha_1\alpha_2 y^3 + 2(1 - 6\alpha_1\alpha_2)y^2 - 4(1 - 3\alpha_1\alpha_2)y + (1 - 4\alpha_1\alpha_2) + \frac{\sigma}{k(\rho_l + \rho_g)\nu^2} = 0, \tag{64}$$

where $\alpha_1=\rho_l/(\rho_l+\rho_g)$, $\alpha_2=\rho_g/(\rho_l+\rho_g)$, and k is the wave number. The root with positive real and imaginary parts is the only physically meaningful solution. The decay rate and oscillating frequency are found from the imaginary and real parts, respectively, of the expression

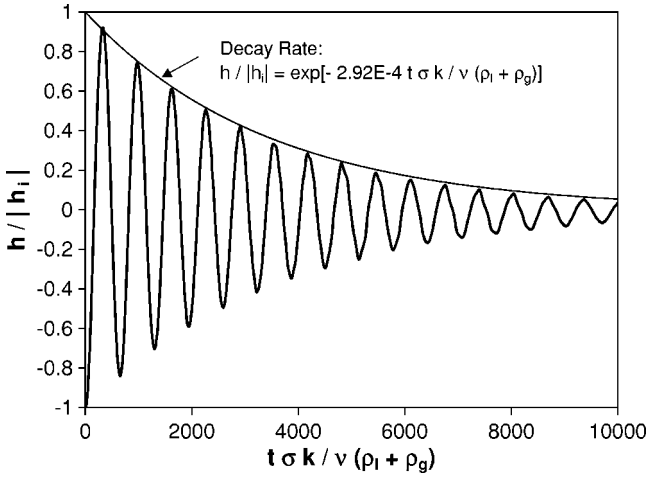

FIG. 4. Oscillation amplitude of a capillary wave versus time using the index function, MRT LBM ($\rho_l=0.2, \rho_g=0.06667, \sigma=0.001\,52, \nu=0.003\,38$).

$$n = (y^2 - 1)\sqrt{\frac{k(\rho_l + \rho_g)\nu^2}{\sigma}}. \tag{65}$$

In the computations, $\rho_l=0.2$, $\rho_g=0.066\,67$, and $k=0.0491$. The viscosity is varied from $\nu=0.1$ to $0.000\,85$, and the surface tension is $\sigma=0.001\,52$ for all computations. The domain size is 129×129. Figure 4 shows the change in amplitude of the capillary wave along with the decay rate when $\nu=0.003\,38$. Figure 5 compares the oscillation frequency and decay rate computed by the index function, MRT LBM, and the index function, BGK LBM [1], to those predicted by Chandrasekhar for the various viscosities versus the ratio of Reynolds to capillary number, $s=\sigma/[k(\rho_l+\rho_g)\nu^2]$. Both models predict the oscillation frequency and decay rate within 8% of their corresponding analytical solu-

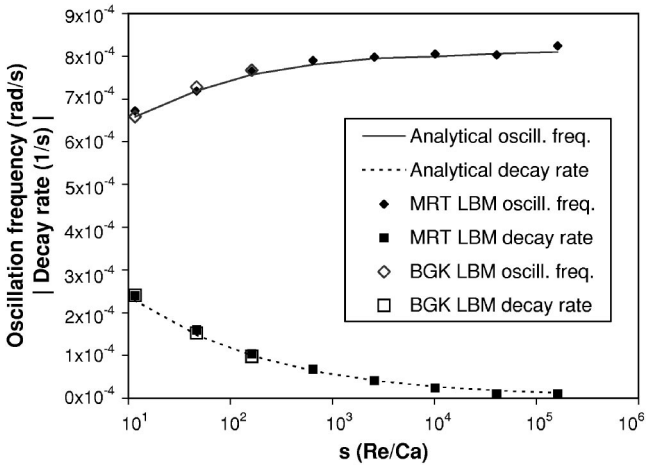

FIG. 5. Oscillation frequency and decay rate versus ratio of Reynolds to capillary numbers.

tions for $s<161$. However, the BGK model is numerically unstable for capillary wave simulations with $\nu \leqslant 0.0135$. The MRT model gives stable solutions for $\nu \geqslant 0.000\,85$ for this computational problem or about a factor of 16 times lower than the BGK model.

VI. DISCUSSION AND CONCLUSIONS

In this paper, we have proposed a MRT LBM model for simulating multiphase flows. The model uses a collision matrix for calculating the effects of collisions in lieu of the single-relaxation-time BGK model. The use of multiple relaxation times allows for different physical quantities to be adjusted independently. It has been suggested that the propagation of sound waves in the BGK model leads to numerical instability. The MRT model has separate adjustable relaxation times for the shear and bulk viscosities as well adjustable parameters for heat flux coefficients. Enhanced numerical stability has been observed by optimally tuning these constants. For ease of use in practical computations, an index function form of the MRT model was also developed. This approach uses one kinetic equation to track the location of liquid in a manner similar to VOF or level sets and another kinetic equation to determine the evolution of pressure and momentum. The MRT model was shown to follow the macroscopic hydrodynamic equations in the macroscopic limit via a multiscale expansion. The index function, MRT model was then evaluated for accuracy on several test problems including Laplace's law for 2D "drops," oscillating liquid cylinders, and capillary waves. The pressure change across the interface of the 2D "drops" was within 6% of the predicted value based upon Laplace's law for most cases. The oscillation frequency of the liquid cylinders was within 4% of the analytical solution for all computations. The capillary wave computations illustrated the enhanced numerical stability of the MRT model compared to the corresponding BGK model in that the MRT model was able to achieve stable results at lower viscosities. Both the MRT and BGK models predicted oscillation frequencies and decay rates within 8% of their analytical values for $s<160$ where s is the ratio of Reynolds to capillary number. The MRT model proposed in this work has been employed to perform initial studies of liquid breakup [21].

ACKNOWLEDGMENTS

The authors thank Dr. Kannan Premnath, Dr. Xiaoyi He, and Dr. Li-Shi Luo for useful discussions during the course of this work. They thank the Purdue University Computing Center for use of their IBM SP and the National Center for Supercomputing Applications (NCSA) for use of their IBM P690.

[1] X. He, S. Chen, and R. Zhang, J. Comput. Phys. **152**, 642 (1999).
[2] X. He, X. Shan, and G. D. Doolen, Phys. Rev. E **57**, R13 (1998).
[3] X. He and G. D. Doolen, J. Stat. Phys. **107**, 309 (2002).
[4] D. Gueyffier *et al.*, J. Comput. Phys. **152**, 423 (1999).
[5] G. Tryggvason *et al.*, J. Comput. Phys. **162**, 708 (2001).
[6] B. Boghosian *et al.*, Proc. R. Soc. London, Ser. A **457**, 717 (2001).
[7] R. Benzi *et al.*, Phys. Rep. **222**, 145 (1992).
[8] I. V. Karlin *et al.*, Europhys. Lett. **41**, 279 (1998).
[9] W.-A. Yong and L.-S. Luo, Phys. Rev. E **67**, 051105 (2003).
[10] P. J. Dellar, Europhys. Lett. **57**, 690 (2002).
[11] P. Lallemand and L.-S. Luo, Phys. Rev. E **61**, 6546 (2000).
[12] P. Lallemand and L.-S. Luo, Phys. Rev. E **68**, 036706 (2003).
[13] D. d'Humieres, in *Rarefied Gas Dynamics: Theory and Simulations*, Progress in Astronautics and Aeronautics, Vol. 159, edited by B. D. Shizgal and D. P. Weaver (AIAA, Washington, D.C., 1992).
[14] J. D. van der Waals, Verhandel. Konink. Akad. Weten. Amsterdam (Sect. 1) **1**(8). 56 (1893).
[15] S. Chapman and T. G. Cowling, *The Mathematical Theory of Non-Uniform Gases*, 3rd ed. (Cambridge University Press, London, 1970).
[16] L.-S. Luo, Phys. Rev. E **62**, 4982 (2000).
[17] T. Lee and C.-L. Lin, Phys. Rev. E **67**, 056703 (2003).
[18] R. Zhang, X. He, and S. Chen, Comput. Phys. Commun. **129**, 121 (2000).
[19] N. Carnahan and K. Starling, J. Chem. Phys. **51**, 635 (1969).
[20] R. Zhang, Ph.D. thesis, University of Delaware, Newark, 2000.
[21] M. McCracken, Ph.D. thesis, Purdue University, West Lafayette, IN, 2004.
[22] D. Rothman and J. Keller, J. Stat. Phys. **52**, 1119 (1988).
[23] A. Gunstensen *et al.*, Phys. Rev. A **43**, 4320 (1991).
[24] X. Shan and H. Chen, Phys. Rev. E **47**, 1815 (1993).
[25] X. Shan and H. Chen, Phys. Rev. E **49**, 2941 (1994).
[26] H. Lamb, *Hydrodynamics* (Cambridge University Press, Cambridge, England, 1932).
[27] K. Nandha Premnath, Ph.D. thesis, Purdue University, West Lafayette, IN, 2004.
[28] S. Chandrasekhar, *Hydrodynamic and Hydromagnetic Stability* (Oxford University Press, Oxford, 1961).